Surface & Coatings Technology 284 (2015) 75–79

Contents lists available at ScienceDirect

Surface & Coatings Technology

journal homepage: www.elsevier.com/locate/surfcoat

Effects of annealing on near-infrared shielding properties of Cs-doped tungsten oxide thin films deposited by electron beam evaporation

Chak Seng Long [a], Horng-Hwa Lu [b,*], Ding-Fwu Lii [c], Jow-Lay Huang [a,d]

[a] Department of Materials Science and Engineering, National Cheng Kung University, Tainan 701, Taiwan
[b] Department of Mechanical Engineering, National Chin-Yi University of Technology, Taichung 41170, Taiwan
[c] Department of Electrical Engineering, Cheng Shiu University, Kaohsiung 833, Taiwan
[d] Department of Chemical and Materials Engineering, National University of Kaohsiung, Kaohsiung 81148, Taiwan

ARTICLE INFO

Article history:
Received 1 April 2015
Revised 6 June 2015
Accepted in revised form 9 June 2015
Available online 26 July 2015

Keywords:
Tungsten bronze
Cs_xWO_3
Near-infrared shielding
Optical properties

ABSTRACT

Near-infrared (NIR) shielding properties are important for solar films. In this study, Cs_xWO_3 films prepared using electron beam evaporation were characterized using X-ray diffraction, X-ray photoelectron spectroscopy, and spectrophotometry. The effects of annealing on NIR shielding properties and film microstructure were investigated. The results show that the NIR shielding properties of Cs_xWO_3 films can be improved by annealing at 300–450 °C under pure H_2 atmosphere, the amorphous thin films being transformed to crystalline films. The Cs_xWO_3 films annealed at 450 °C in pure H_2 atmosphere showed high transmittance of visible light (70%) and high NIR shielding ratio (99%).

1. Introduction

Near-infrared (NIR) light shielding materials have been applied in solar collectors, smart windows, and optical filters [1–3]. NIR shielding has been achieved by utilizing transparent thermal coatings on windows. In summer, transparent thermal insulation coatings, which have excellent visible light transmittance, prevent heat transmission from the outside to the inside reducing air conditioning usage and, thus, energy consumption [4,5]. Transparent thermal insulation coatings can also be used as a solar filter. Transparent conductive oxides (TCOs) include indium tin oxide (ITO) and antimony tin oxide (ATO) [6]. Tungsten bronzes have received a lot of attention due to their electrochromic, photochromic, gasochromic, and superconducting properties [7–11]. Tungsten bronzes M_xWO_3 with dopant ions such as Na, K, Rb, Cs, and other alkali metals [12,13] have been found to have the best optical and electrical properties. Takeda et al. [14] found that cesium tungsten bronze (Cs_xWO_3) film has excellent NIR absorption and shielding properties. One study [15] found that Cs_xWO_3 has a strong NIR shielding ability as well as high transparency in the visible light region. Cs_xWO_3 with a hexagonal structure exhibited higher NIR shielding than that of ITO, and is thus a possible replacement for ITO and ATO in windows. Cs_xWO_3 powders have mainly been synthesized via the solvothermal reaction method [16–18] or hydrothermal reaction method [19–21] before being coated onto substrates. The present study is aimed at the investigation of the H_2 annealing effects on the microstructure, morphology and NIR shielding properties of the Cs_xWO_3 films prepared by electron beam evaporation.

2. Experimental Procedure

Thin films of Cs_xWO_3 were deposited on quartz glass via electron beam evaporation. The source material was Cs_xWO_3 ($0 < x < 1$) powders. (NanoStar Technology Co). The substrates were cleaned with acetone and methanol by treatment for 10 min in each solvent. Then, the substrates were washed with isopropyl alcohol and deionized water for 10 min. The electron gun was operated at 8 kV and 10 mA. The evaporation was carried out for 40 min at a base pressure of 7.5×10^{-6} Torr. The films were grown at a constant temperature (273 K). The thickness of the Cs_xWO_3 films was controlled to be 280 nm with deposition at a constant rate of 3 Å · s^{-1} using an in situ quartz crystal thickness monitor. The phase composition and crystallinity of the Cs_xWO_3 film were determined using X-ray diffraction (XRD) analysis (Rigaku DMAX 2500) with Cu Kα radiation ($\lambda = 1.54$ Å) at a scan speed of 1°/min. Ultrahigh-resolution field-emission scanning electron microscopy (UHRFE -SEM; ZEISS SUPRA series) and energy-dispersive X-ray spectroscopy (EDX) analysis were performed. The binding energies of tungsten core levels in the Cs_xWO_3 film were determined using X-ray photoelectron spectroscopy (XPS; VersaProbe PHI 5000). The morphology of the film was determined using field-emission SEM (Hitachi-4800). The optical transmittance spectra were measured at room temperature (RT) using ultraviolet/visible/NIR spectrophotometry

* Corresponding author.
E-mail address: hhlu@ncut.edu.tw (H.-H. Lu).

http://dx.doi.org/10.1016/j.surfcoat.2015.06.078
0257-8972/

(Hitachi U-4100) in the wavelength range of 260-2600 nm. The surface morphology of the deposited film was observed using atomic force microscopy (AFM; Veeco CP-II) in semi-contact mode with Si tips at a scan rate of 1 Hz.

3. Results and Discussion

3.1. Microstructure of films

Fig. 1 shows SEM images of Cs_xWO_3 thin films before and after H_2 annealing at 300-500 °C. No obvious precipitates or impurities appear on the surface of the $Cs_{0.32}WO_3$ thin films (Fig. 1(a)). Fig. 1(b) and (c) show no distinct variation in the surface morphology of the thin films after annealing. However, when the annealing temperature was 400 °C, the grain size increased (Figs. 1(d) and (e)).

Fig. 2 shows three-dimensional (3D) AFM images (scanning area: 3 μm × 3 μm) of Cs_xWO_3 thin films deposited at various annealing temperatures. The films deposited at RT had a relatively smooth surface with vague grain boundaries, as shown in Fig. 2(a). The roughness was found to be 0.95 nm and the surface was continuous. The surface roughness and grain size increased with increasing annealing temperature. As shown in Figs. 2(b) and (c), when the annealing temperature was increased from 300 to 350 °C, the surface roughness increased from 1.55 to 1.73 nm. The surface roughness increased from 2.15 nm (400 °C) to 4.77 nm (450 °C). The grain size increase with annealing temperature is attributed to atomic rearrangement (atoms move faster on the surface of the films at higher temperature).

3.2. Phase composition of films

Fig. 3 shows XRD patterns of Cs_xWO_3 thin films before and after H_2 annealing at 300-450 °C for 2 h. Fig. 3(a) shows XRD patterns of as-deposited $Cs_{0.32}WO_3$ thin films. The diffraction peak absence indicates the amorphous film state. Figs. 3 (b-e) show XRD patterns of films annealed at 300, 350, 400, and 450 °C for 2 h, respectively. The Cs_xWO_3 thin film crystallization is found after treatment at 300 °C. The characteristic peaks of the Cs_xWO_3 thin films corresponded to the (002), (200), (112), (202), (212), (220), (204), (312), (400), and (224) planes. This agrees well with hexagonal $Cs_{0.32}WO_3$ (JCPDS card no. 831334). No impurity peaks appeared. With increasing annealing temperature, the diffraction peaks became more apparent and sharper. It was reported that Cs ions (0.170 nm) can occupy hexagonal vacant tunnels (0.163 nm) in the hexagonal tungsten bronze structure [1]. The grain size, D, of the crystallites was calculated using Scherrer's formula:

$$D = \frac{K\lambda}{\beta \cos\theta}$$

where K is the Scherrer constant (= 0.9), λ is the wavelength of the X-ray (= 1.54 Å for Cu Kα radiation), θ is the Bragg angle, and β is the line broadening at half the maximum intensity (full width at half maximum). The grain size, D, increased from 15 to 30 nm when the annealing temperature was increased from 0 to 400 °C. The initially amorphous $Cs_{0.32}WO_3$ thin films gradually crystallized with increasing H_2 annealing temperature. This result is consistent with the SEM and AFM images in Figs. 1 and 2.

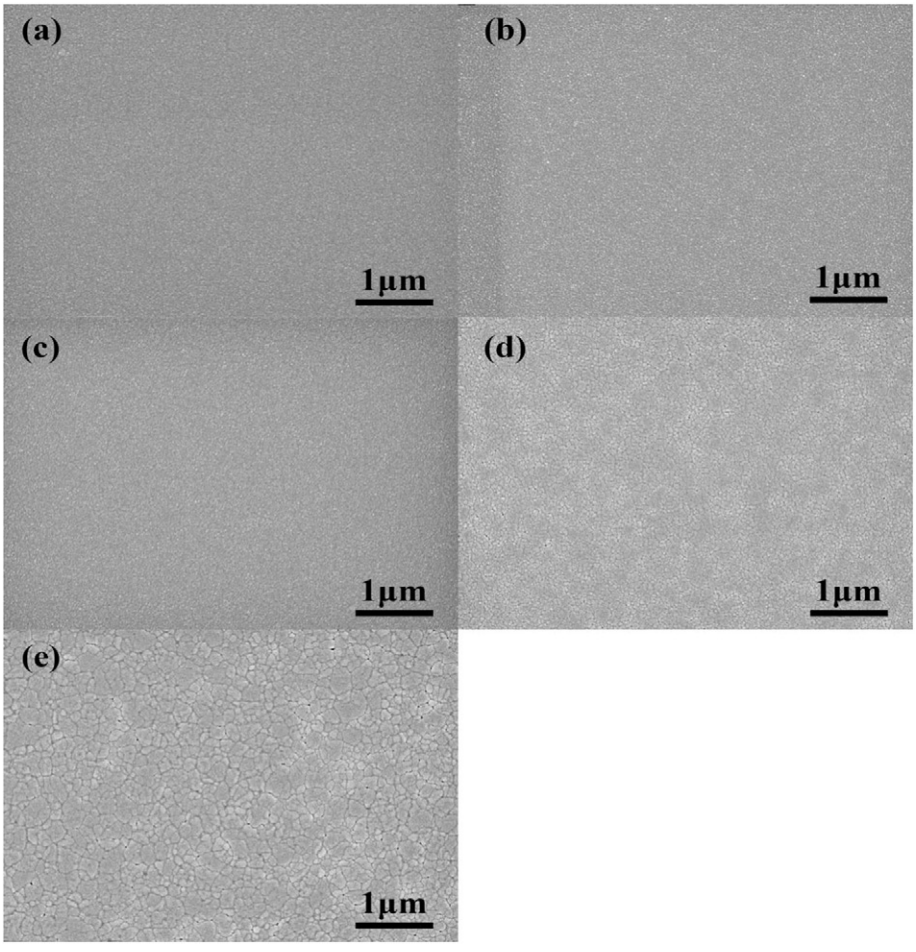

Fig. 1. SEM images of (a) as-sputtered $Cs_{0.32}WO_3$ films and those annealed at (b) 300 °C, (c) 350 °C, (d) 400 °C, and (e) 450 °C.

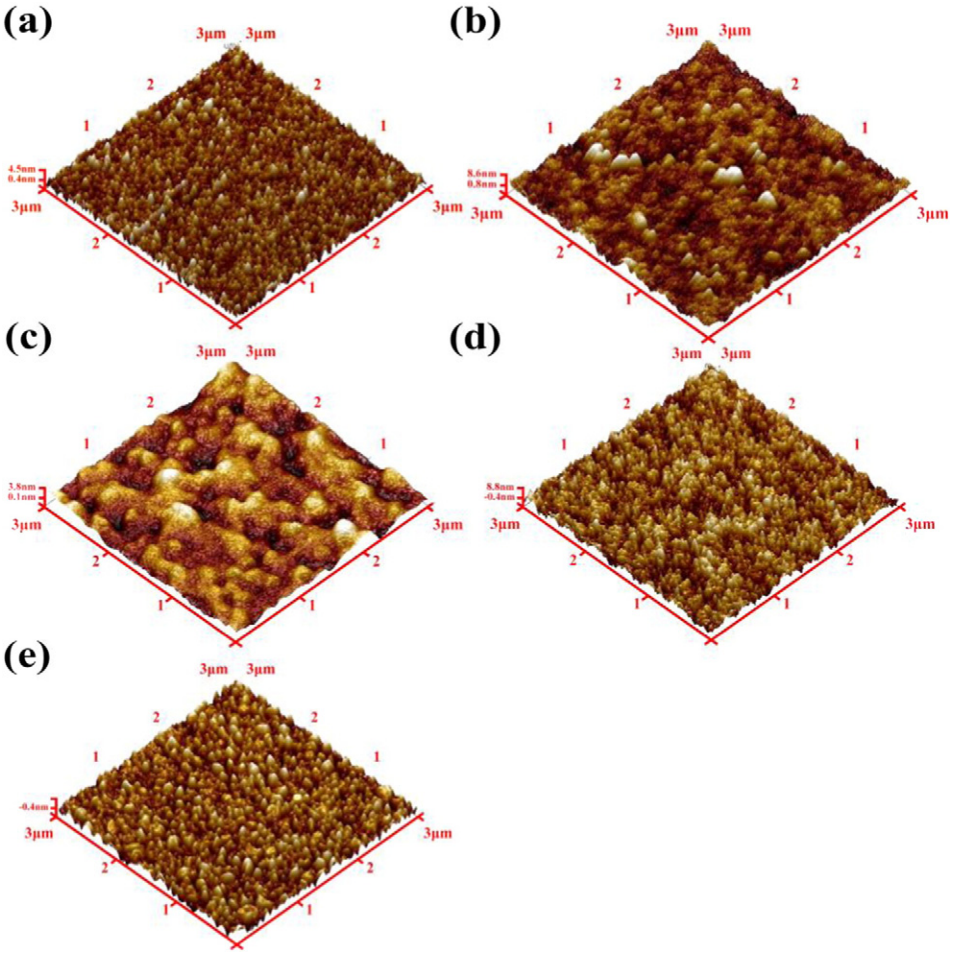

Fig. 2. 3D AFM images of (a) as-deposited $Cs_{0.32}WO_3$ thin films and those annealed at (b) 300 °C, (c) 350 °C, (d) 400 °C, and (e) 450 °C.

The EDX spectra of the Cs_xWO_3 thin films are shown in Fig. 4. Fig. 4(a) shows peaks corresponding to W and O, with no Cs on the surface, because of local area. Fig. 4(b) shows peaks corresponding to W, Cs, and O, indicating the possible formation of Cs_xWO_3 on the surface.

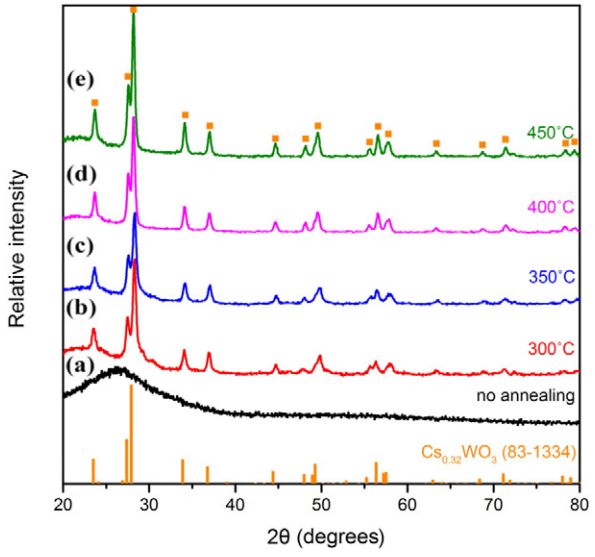

Fig. 3. XRD patterns of Cs_xWO_3 thin films deposited on quartz glass substrates via electron beam evaporation: (a) as- deposited $Cs_{0.32}WO_3$ thin films and annealed at (b) 300 °C, (c) 350 °C, (d) 400 °C, and (e) 450 °C.

Table 1 displays the element analysis results of the Cs_xWO_3 before and after H_2 annealing at different temperature by XPS. It can be found that as-deposited Cs_xWO_3 thin film exhibits the minimum Cs/W

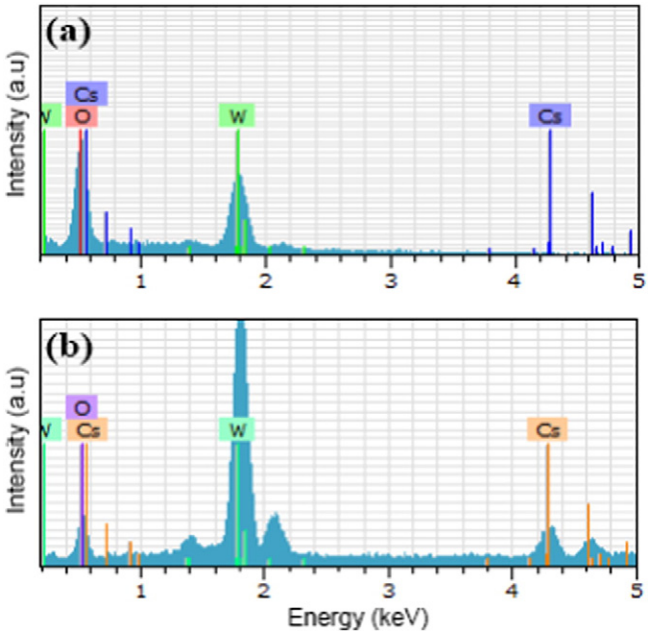

Fig. 4. EDX spectra of (a) as-sputtered film and (b) films annealed at above 300 °C.

Table 1
The XPS analysis of Cs_xWO_3 before and after H_2 annealing at different temperatures.

Sample	Element concentration (%)				O/W atomic ratio	Cs/W atomic ratio	Composition
	C_{1s}	O_{1s}	Cs_{3d}	W_{4f}			
No H_2 annealing	50.6	33.0	4.3	12.1	2.73	0.36	$Cs_{0.36}WO_{2.73}$
H_2-300°C	29.6	47.3	7.1	16.0	2.96	0.44	$Cs_{0.44}WO_{2.96}$
H_2-350°C	31.5	44.8	8.6	15.2	2.95	0.57	$Cs_{0.57}WO_{2.95}$
H_2-400°C	30.1	46.8	9.0	14.1	3.32	0.64	$Cs_{0.64}WO_{3.32}$
H_2-450°C	25.4	47.5	11.2	15.9	2.99	0.70	$Cs_{0.7}WO_{2.99}$

atomic ratio, which indicate the thin films existence of Cs element. Furthermore, the thin films after annealed at 300-450 °C exhibit higher Cs/W atomic ratio. This result is entirely consistent with previous studies [16].

Fig. 5(a) shows the W 4f doublet of the Cs_xWO_3 thin films before and after H_2 annealing, as obtained from XPS. The peaks of the W_{4f} core-level spectra of the as-sputtered film are located at 35.1 and 37.2 eV [22]. The two peaks of W_{4f} show a shift to higher binding energies after H_2 annealing, which indicates that the chemical state of W changed due to the Cs-deficient surface of the Cs_xWO_3 thin films after the reduction reaction. However, excess oxygen deficiencies remained on the surface. Cs^+ ions diffused from the inside of the $Cs_{0.32}WO_3$ thin films to the surface during H_2 annealing [23]. Fig. 5(b) shows the W_{4f} XPS spectra of the thin films after H_2 annealing at 450 °C for 1 h. The W_{4f} core-level spectra can be fitted as two spin-orbit doublets, $W_{4f7/2}$ and $W_{4f5/2}$, for the interval of about 2.1 eV. The peaks of the first doublet, located at 35.2 and 37.3 eV, are attributed to W^{6+} and those of the second doublet, located at 34 and 36.1 eV, are attributed to W^{5+}. The chemical state of W changed due to the partial reduction of W^{6+}. This suggests that the non-stoichiometric cesium tungsten bronzes Cs_xWO_3 are reduced compounds, which can be expressed by the general formula $Cs_xW_x^{5+}W_{1-x}^{6+}O_3$.

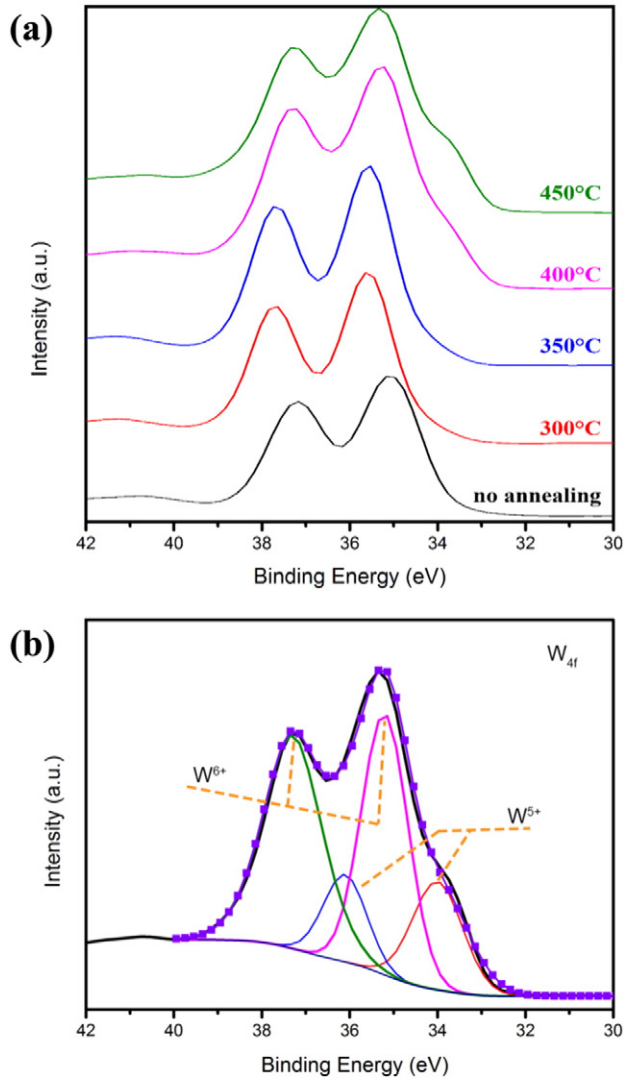

Fig. 5. XPS spectra of Cs_xWO_3 films prepared via electron beam evaporation: (a) as-sputtered and annealed at various temperatures and (b) 450 °C for 1 h.

3.3. Optical properties of films

Fig. 6 shows the transmittance spectra of $Cs_{0.32}WO_3$ thin films on quartz glass substrates before and after annealing at various temperatures. Fig. 6(a) shows that the $Cs_{0.32}WO_3$ thin films before annealing are highly transparent in both the visible and NIR regions due to the wide band gap and lack of free electrons [24]. Figs. 6(b) and (c) show that the films are transparent pale blue and have more than 80% transmittance in the visible region. The films have high NIR light shielding performance as well as high transparency for visible light. When the annealing temperature was 400 °C, the transmittance was about 70% and also decrease in the NIR region, respectively. This indicates that the $Cs_{0.32}WO_3$ thin films after annealing at 400-450 °C have better NIR shielding properties than those of films annealed at 300-350 °C. The sample annealed at 450 °C showed excellent NIR shielding ability as well as high transparency in the visible light region. The NIR shielding ability of the films is higher than that of ITO glass. This result indicates that $Cs_{0.32}WO_3$ thin film is a promising heat shielding material that can replace ITO and ATO. A previous study [25] reported that $Cs_{0.32}WO_3$ thin films realized stronger absorption properties of the NIR light rather than reflection. It has been suggested that NIR absorption is related to the plasmon resonance of free electron interband transition and small polarons [26,27]. The reduction of the film transmittance is due to the oxygen deficiency occurred at high annealing temperatures.

4. Conclusion

Cs_xWO_3 thin films were prepared via electron beam evaporation and annealed in an H_2 atmosphere. The effects of annealing on the microstructure and NIR shielding properties of the Cs_xWO_3 thin films were investigated. The films grown at RT were amorphous. Crystalline films were obtained at annealing temperatures of above 300 °C. The film color changed from pale yellow to deep blue with increasing annealing

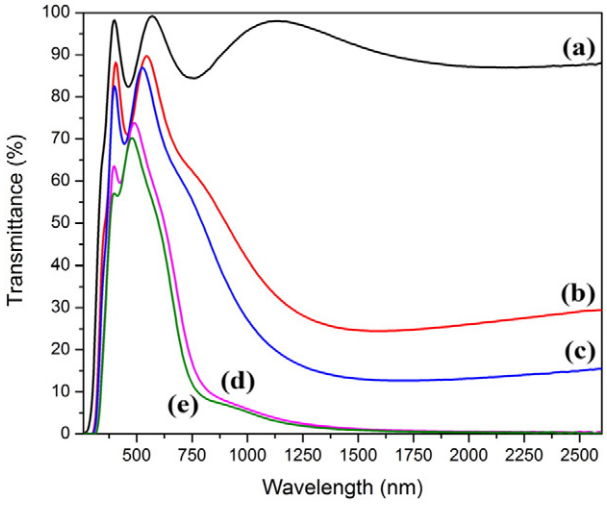

Fig. 6. Transmission spectra of $Cs_{0.32}WO_3$ thin films: (a) as-sputtered and annealed at (b) 300 °C, (c) 350 °C, (d) 400 °C, and (e) 450 °C.

temperature. The grain size and surface roughness of the films increased with increasing annealing temperature. The NIR shielding properties of Cs_xWO_3 films were improved by annealing at 300-450 °C under a pure H_2 atmosphere, with the amorphous thin films transforming into crystalline films. With annealing at 450 °C, Cs_xWO_3 films showed the best NIR shielding properties, with a high transmittance of visible light (70%) and a high NIR shielding ratio (99%).

Acknowledgments

This project was financially supported by the Ministry of Education of the ROC under contract No. 102E-70-001.

References

[1] C.S. Guo, S. Yin, M. Yan, T. Sato, J. Mater. Chem. 21 (2011) 5099.
[2] C. Guo, S. Yin, P. Zhang, M. Yan, K. Adachi, T. Chonan, T. Sato, J. Mater. Chem. 20 (2010) 8227–8229.
[3] C. Guo, S. Yin, L. Huang, L. Yang, T. Sato, Chem. Commun. 47 (2011) 8853–8855.
[4] M. Okada, Y. Yamada, P. Jin, M. Tazawa, K. Yoshimura, Thin Solid Films 442 (2003) 217–221.
[5] C. Guo, S. Yin, L. Huang, T. Sato, ACS Appl. Mater. Interfaces 3 (2011) 2794–2799.
[6] E. Elangovan, S.A. Shivashankar, K. Ramamurthi, J. Cryst. Growth 276 (2005) 215–221.
[7] S.J. Yoo, Y.H. Jung, J.W. Lim, H.G. Choi, D.K. Kim, Y.E. Sung, Sol. Energy Mater. Sol. Cells 92 (2008) 179–183.
[8] C.H. Rüscher, K.R. Dey, T. Debnath, I. Horn, R. Glaum, A. Hussain, J. Solid State Chem. 181 (2008) 90–100.
[9] G. Urretavizcaya, F. Tonus, E. Gaudin, J.L. Bobet, F.J. Castro, J. Solid State Chem. 180 (2007) 2785–2789.
[10] J. Guo, C. Dong, L. Yang, G. Fu, H. Chen, Mater. Res. Bull. 42 (2007) 1384–1389.
[11] R.K. Stanley, R.C. Morris, W.G. Moulton, Phys. Rev. B 20 (1979) 1903–1914.
[12] C.S. Guo, S. Yin, T. Sato, J. Am. Ceram. Soc. 95 (2012) 1634–1639.
[13] M.R. Skokan, W.G. Moulton, R.C. Morris, Phys. Rev. B 20 (1979) 3670–3677.
[14] H. Takeda, K. Adachi, J. Am. Ceram. Soc. 90 (2007) 4059–4061.
[15] G.X. Liu, S.N. Wang, Y.T. Nie, X.H. Sun, Y.H. Zhang, Y. Tang, J. Mater. Chem. A 1 (2013) 10120–10129.
[16] J.X. Liu, F. Shi, X.L. Dong, Q. Xu, S. Yin, T. Sato, Mater. Charact. 84 (2013) 182–187.
[17] J.X. Liu, Y. Ando, X.L. Dong, F. Shi, S. Yin, K. Adachi, T. Chonan, A. Tanaka, T. Sato, J. Solid State Chem. 183 (2010) 2456–2460.
[18] J.-X. Liu, F. Shi, X.-L. Dong, S.-H. Liu, C.-Y. Fan, S. Yin, T. Sato, Powder Technology, Part A 270 (2015) 329–336.
[19] F. Shi, J.X. Liu, X.L. Dong, Q. Xu, J.Y. Luo, H.C. Ma, J. Mater. Sci. Technol. 30 (2014) 342–346.
[20] J. Liu, J. Luo, F. Shi, S. Liu, C. Fan, Q. Xu, G. Shao, J. Solid State Chem. 221 (2015) 255–262.
[21] J. Liu, Q. Xu, F. Shi, S. Liu, J. Luo, L. Bao, X. Feng, Appl. Surf. Sci. 309 (2014) 175–180.
[22] J. Li, Y. Liu, Z. Zhu, G. Zhang, T. Zou, Z. Zou, S. Zhang, D. Zeng, C. Xie, Sci. Rep. 3 (2013) 2409.
[23] K. Adachi, Y. Ota, H. Tanaka, M. Okada, N. Oshimura, A. Tofuku, J. Appl. Phys. 114 (2013) 194304.
[24] C. Guo, S. Yin, Q. Dong, T. Sato, CrystEngComm 14 (2012) 7727.
[25] C.-J. Chen, D.-H. Chen, Nanoscale Res. Lett. 8 (2013) 1–8.
[26] D.W. Lynch, R. Rosei, J.H. Weaver, C.G. Olson, J. Solid State Chem. 8 (1973) 242–252.
[27] O.F. Schirmer, V. Wittwer, G. Baur, G. Brandt, J. Electrochem. Soc. 124 (1977) 749–753.